Supplementary Information

CK2 signaling from TOLLIP-dependent perinuclear endosomes is an essential feature of *KRAS* mutant cancers

Srikanta Basu, Brian T. Luke, Baktiar Karim, Nancy Martin, Stephen Lockett, Sudipto Das, Thorkell Andresson, Karen Saylor, Serguei Kozlov, Laura Bassel, Dominic Esposito, and Peter F. Johnson

Extended Data Figure 1

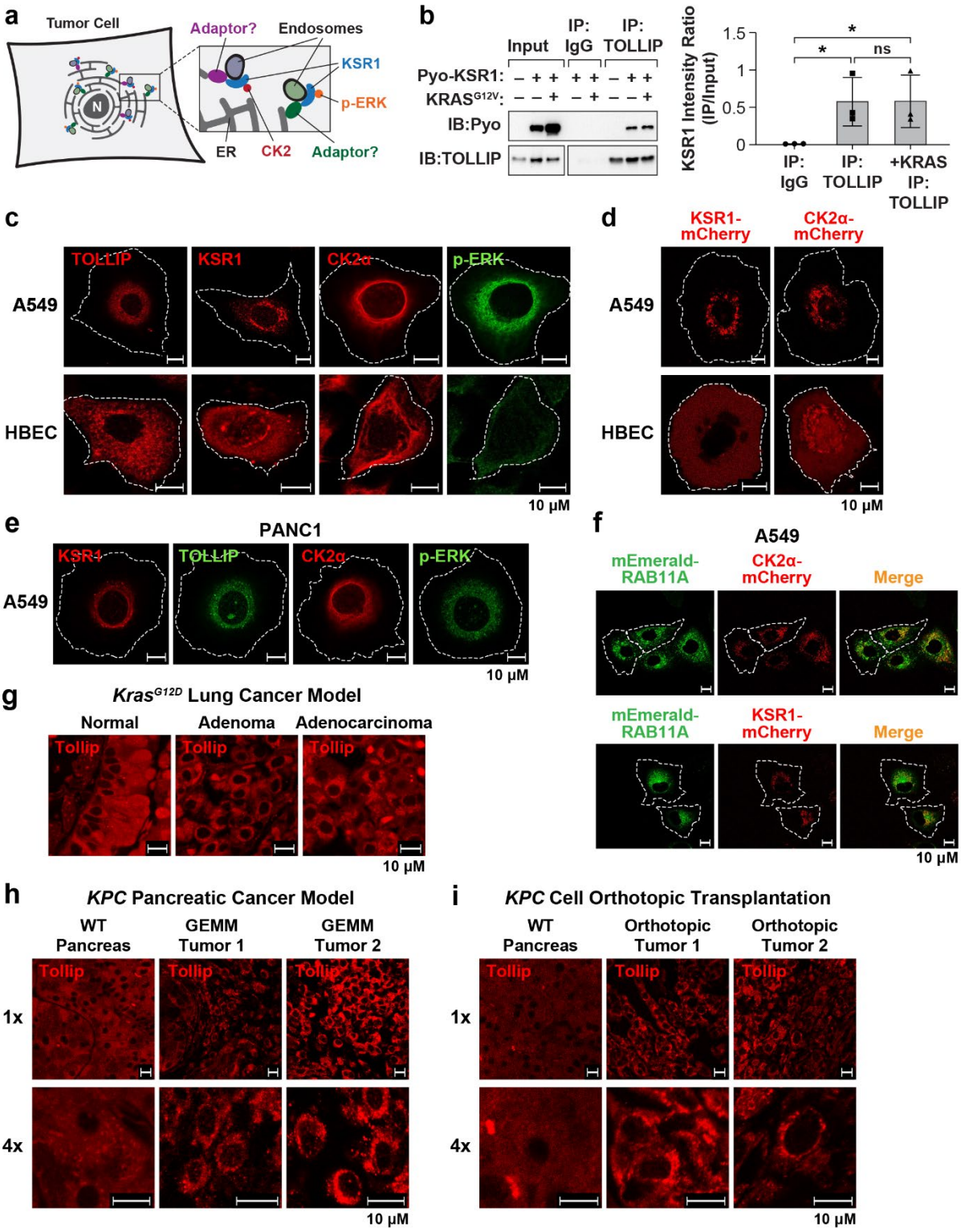

Extended Data Fig. 1 | Perinuclear TOLLIP corresponds to the presence of PSCs in tumor cell lines and tissues. a, A model for recruitment of signaling endosomes to the perinuclear ER network by adaptor proteins. CK2 and ERK are present on different types of signaling endosomes that may use distinct adaptor proteins for attachment to the ER. **b**, IP experiment showing endogenous TOLLIP associating with ectopically expressed Pyo-KSR1 in 293T cells. The graph shows quantitative data for three experiments. **c**, IF imaging demonstrating perinuclear clustering of TOLLIP, KSR1, CK2a and p-ERK in A549 cells and dispersed cytoplasmic patterns in HBEC cells. **d**, Fluorescently tagged KSR1 and CK2a are perinuclear in A549 cells, in contrast to pan-cytoplasmic distribution in non-transformed HBEC cells. **e**, TOLLIP, CK2a and p-ERK segregate to the nuclear-proximal region in *KRAS* mutant PANC1 PDAC cells. **f**, Live cell imaging showing partial co-localization of fluorescently tagged RAB11A with CK2a and KSR1 in A549 cells. **g**, Tollip is perinuclear in $Kras^{G12D}$-driven lung adenomas and ADCs but displays diffuse staining in unaffected normal lung tissue. **h**, Tollip forms perinuclear rings in primary PDAC tumors arising in *KPC* mice and pan-cytoplasmic distribution in normal pancreas. **i**, Tollip displays perinuclear staining in pancreatic tumors from orthotopic *KPC* cell allografts compared with uniform distribution in normal host pancreas.

Statistical significance for quantitation of immunoprecipitation was calculated using Student's t test; * $p \leq 0.05$.

Extended Data Figure 2

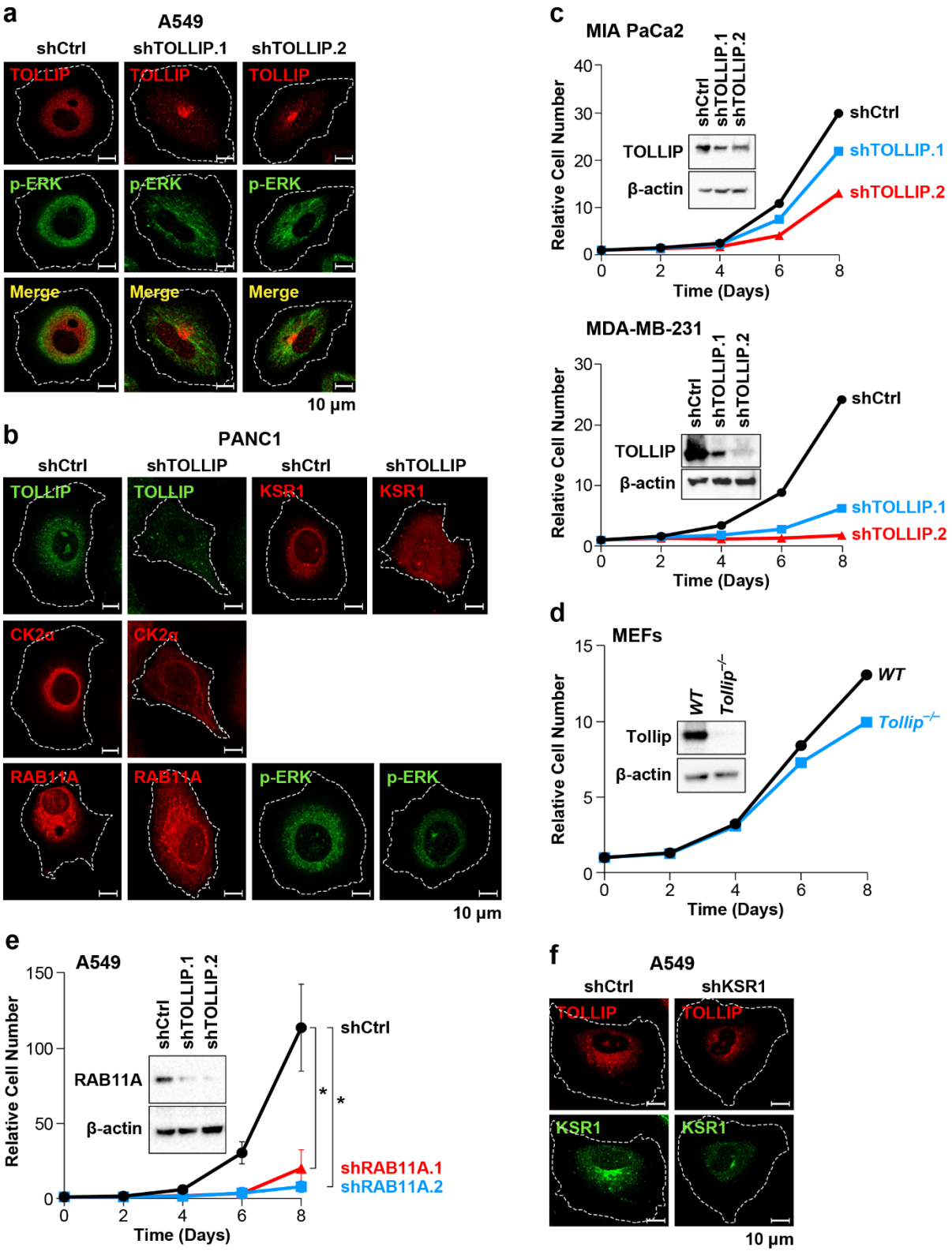

Extended Data Fig. 2 | a, TOLLIP depletion in A549 cells does not alter perinuclear localization of p-ERK. **b**, TOLLIP silencing alters perinuclear localization of CK2α, KSR1 and RAB11A but not p-ERK in PANC1 cells (*KRAS*^{G12C} PDAC). **c**, TOLLIP depletion decreases proliferation of the tumor cell lines MIA PaCa-2 (*KRAS*^{G12C} PDAC) and MDA-MB-231 (*KRAS*^{G13D} breast cancer). **d**, *Tollip* knockout MEFs proliferate similarly to *WT* cells. **e**, RAB11A silencing impairs proliferation of A549 cells. **f**, A549 cells depleted for KSR1 retain nuclear proximal localization of TOLLIP. Two-way ANOVA was used to analyze growth curves; * $p \leq 0.05$.

Extended Data Figure 3

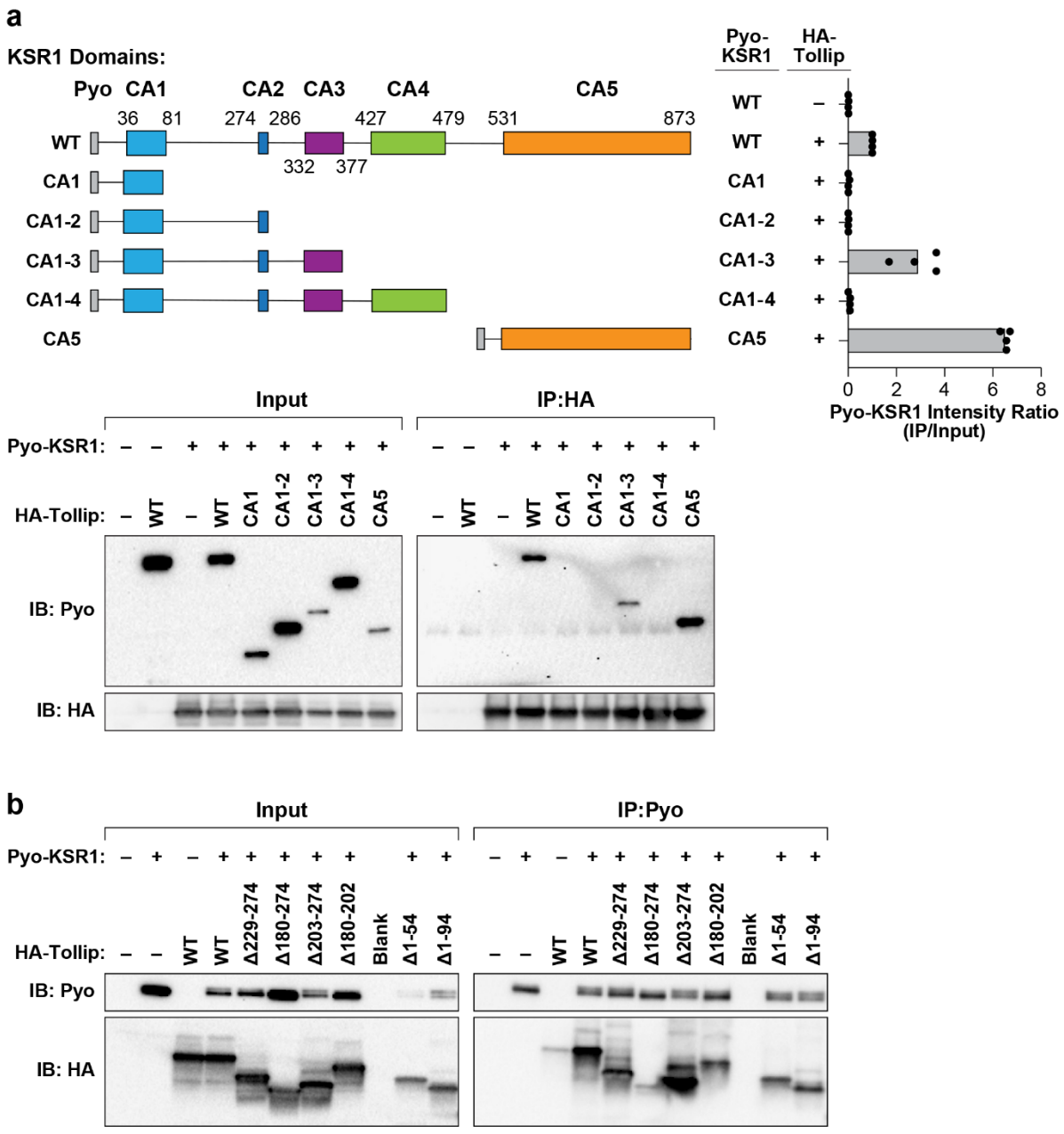

Extended Data Fig. 3 | Mapping interaction domains and functional regions in KSR1 and Tollip. a, The conserved KSR1 CA5 (pseudokinase) domain predominantly mediates association with Tollip. Nested KSR1 C-terminal deletions were generated to map the Tollip binding region. Conserved regions CA1-CA5 along with the endpoint of each deletion are depicted, with a Pyo tag appended to the N termini. CA5 alone was also tested. KSR1 proteins were co-expressed with HA-Tollip in HEK293T cells and lysates were immunoprecipitated using HA antibody. Input lysates and IP samples were analyzed by immunoblots probed for HA or Pyo (lower panel). Band intensities were quantified, and IP/input ratios determined for each KSR1 protein (upper right); values are normalized to WT KSR1. Means ± s.d.; n=3 independent experiments. **b**, Immunoblot showing HA-Tollip mutants (see Fig. 3a) co-immunoprecipitating with Pyo-KSR1.
Student's t-test was performed for IP quantification; * $p \leq 0.05$.

Extended Data Figure 4

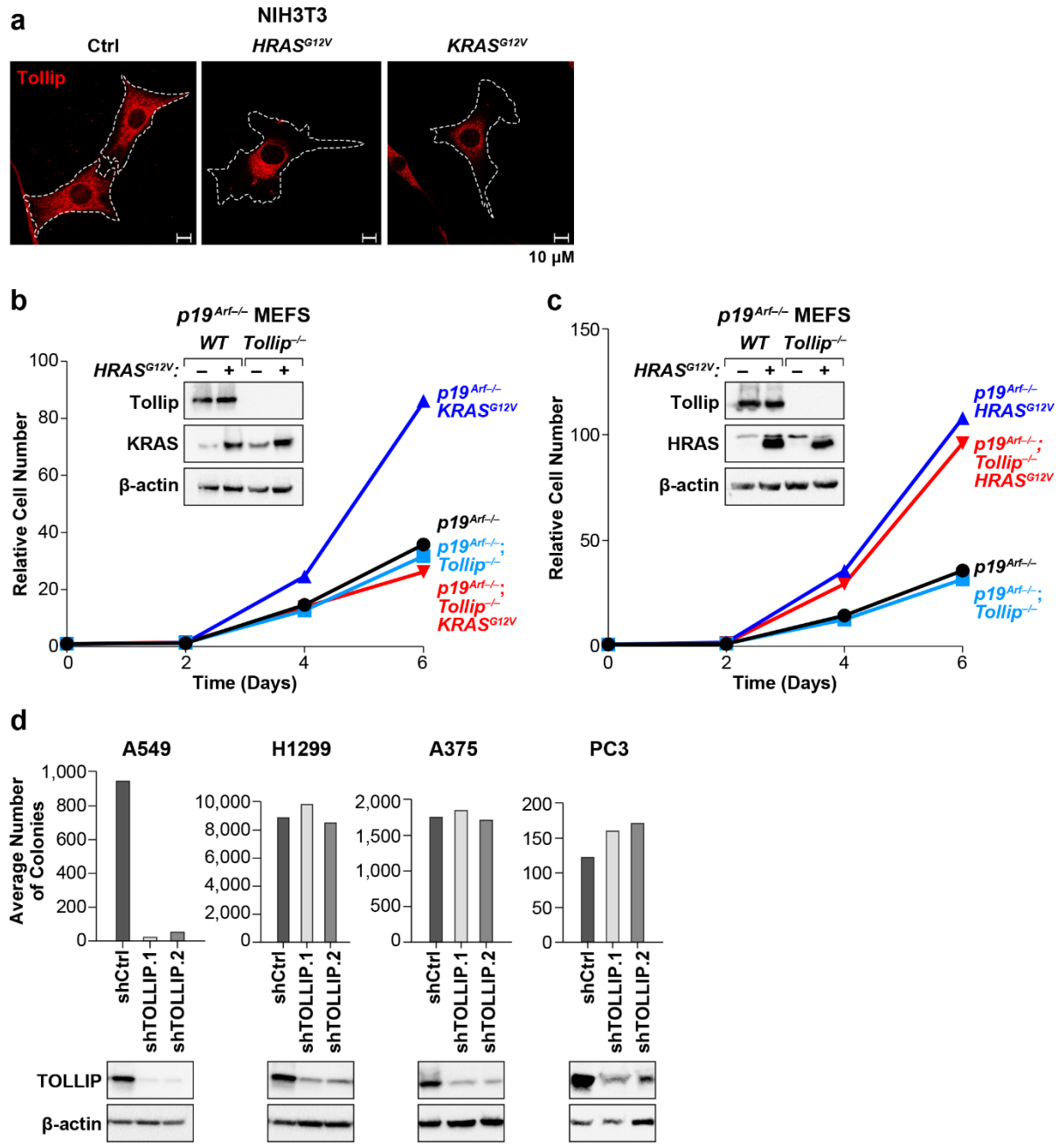

Extended Data Fig. 4 | Tumor cells harboring non-*KRAS* oncogenes do not require Tollip for proliferation/survival. a, Oncogenic *KRAS* and *HRAS* induce perinuclear localization of Tollip in NIH3T3 cells. **b**,**c**, $p19^{Arf-/-}$ MEFs require Tollip for $KRAS^{G12V}$-driven but not $HRAS^{G12V}$-induced hyperproliferation. **d**, Human tumor cells carrying oncogenic mutations in *NRAS* (H1299 lung ADC, $NRAS^{Q61K}$), *BRAF* (A375 melanoma, $BRAF^{V600E}$), or *PTEN* (PC3 prostate cancer, *PTEN* null) are unaffected by TOLLIP depletion in clonogenic growth assays. A549 cells are included for comparison.

Two-way ANOVA was used to analyze growth curves. Student's t-test was performed for colony formation assays; * $p \leq 0.05$.

Extended Data Figure 5

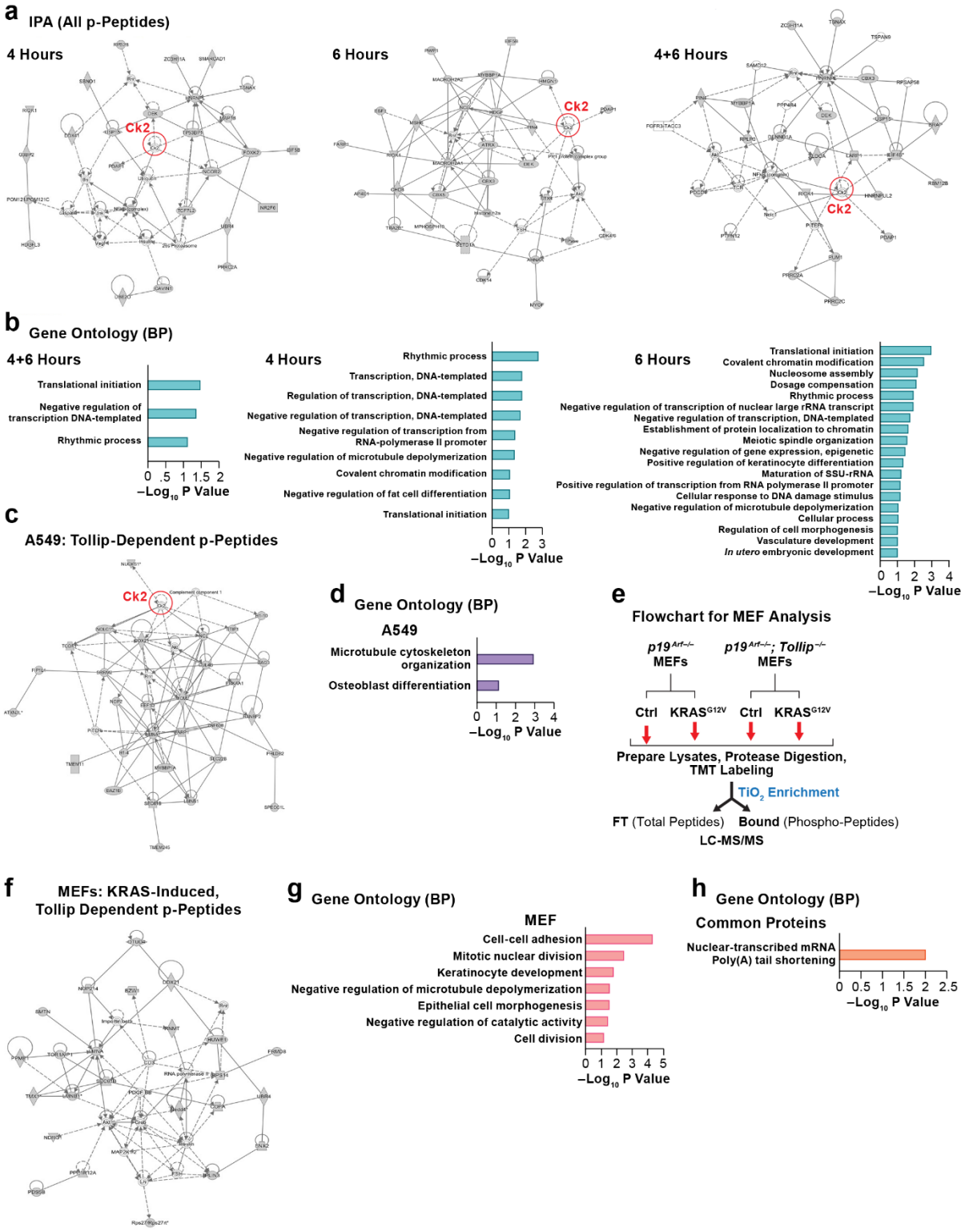

Extended Data Fig. 5 | Bioinformatic analysis of phosphoproteomic data. a, Ingenuity Pathways Analysis (IPA) of signaling networks corresponding to p-peptides from serum-stimulated NIH3T3 cells. Data from all p-peptides (4 h, 6 h or 4+6 h) was used for the analysis. The highest-scoring network is shown for each data set, and CK2 nodes are indicated by red circles. **b**, Ranked GO terms for proteins corresponding to p-peptides (CK2 sites) increased at 4 and/or 6 h (DAVID, biological process). The most significant GO terms are presented, with data plotted as $-\log_{10}$(Pvalue). **c**, Gene ontology analysis (DAVID, biological process) of proteins corresponding to CK2 site p-peptides that decrease in TOLLIP-depleted A549 cells. **d**, IPA signaling network for all p-peptides selectively decreased in TOLLIP-depleted A549 cells. A CK2 node is highlighted by the red circle. **e**, Scheme for generating *KRAS*-induced phosphoproteomes in *WT* and *Tollip*$^{-/-}$ MEFs. **f**, IPA signaling network for all p-peptides preferentially induced by *KRAS* in *WT* vs. *Tollip*$^{-/-}$ MEFs. **g**, Gene ontology analysis (DAVID, biological process) of proteins corresponding to CK2 site p-peptides preferentially induced by *KRAS*^{G12V} in *WT* vs. *Tollip*$^{-/-}$ MEFs. **h**, Ranked GO terms (DAVID, biological process) for the set of common proteins corresponding to CK2 site p-peptides in at least 2 out of 3 data sets (NIH3T3, MEFs and A549 cells).